Blade Torsional Tuning to Manage Large Amplitude Control Loads

R. Gabel* and F. Tarzanin Jr.†
Boeing Vertol Company, Philadelphia Pa.

Helicopter flight envelope growth is currently limited by large amplitude control loads. A systematic study with current tools shows that selection of the rotor blade torsional natural frequency has the potential for reducing the large loads, making further flight envelope growth possible. For the blade studies, the maximum control load occurred at torsional natural frequencies from 7.5/rev to 9.5/rev; and higher or lower torsional frequencies reduced the load. Torsional frequency variations due to changes in blade stiffness, control system stiffness, and pitch inertia yielded similar results, theoretically verifying that blade torsional frequency is a primary variable. A preliminary test of blade torsional stiffness variation confirmed the theoretical trend, but these results are only tentative because the model configuration did not permit constant propulsive force during the test.

Nomenclature

C_L = airfoil lift coefficient
C_M = airfoil pitching moment coefficient at the quarter chord
C_T/σ = nondimensional rotor thrust, based on rotor thrust divided by solidity
GJ = torsional rigidity
H_D = density altitude, ft
K_Z = control system linear spring rate
L = aerodynamic lift
PA = pitch axis location, percent of chord aft of the leading edge
T/P = test point number
V_0 = aircraft forward speed
V = local wind velocity
$\bar{X}$ = nondimensional propulsive force
α = airfoil angle of attack
μ = advance ratio
$\theta_{0.75}$ = blade element collective angle at 75% span
ω_θ = rotor blade torsional natural frequency
$\dot{\alpha}$ = time derivative of the angle of attack

Introduction

A MAJOR design objective is to produce an aircraft with a flight envelope limited by aircraft power and not by structural limits. However, a prime limitation to the operational flight envelope of helicopters has been the rapid growth of control loads that exceed the endurance limit with increased airspeed, gross weight, or altitude. These large loads limit the flight envelope so that the available power cannot be fully utilized.

The large control loads are attributed to 'stall flutter' which is a consequence of high angles of attack and the resulting retreating blade stall. Visual confirmation of stall flutter can be found in pitch link or blade torsional gage waveforms on which characteristic stall spikes appear in the fourth quadrant of the blade azimuth. These high loads result from an aeroelastic self-excited pitching motion in conjunction with repeated submersion of a large portion of the rotor blade into and out of stall. Helicopter stall flutter is a limit-cycle oscillation that occurs, strictly speaking, only in hover. In forward flight, blade stall and the corresponding large torsional loads occur for only a fraction of the rotor cycle. In neither hover nor forward flight does the phenomenon become divergent, but it does cause extremely large torsional loads.

Analytical investigations into the stall flutter phenomenon are aimed at finding methods for reducing or eliminating the large torsional moments and control system loads. Possible methods for reducing these loads include: structural blade variations, control system modifications, and aerodynamic changes. Limited analytical studies of the effect of control system stiffness by Boeing-Vertol and Sikorsky Aircraft,[1,2] have indicated that reducing the blade torsional natural frequency reduced stall flutter control loads. This paper reports an extensive theoretical study that evaluates the effects of torsional stiffness, control system stiffness, and pitch inertia on a highly loaded (C_T/σ = 0.114) full scale rotor at an advance ratio of 0.29. The analytical results showed that large reduction in stall flutter loads can be achieved. These encouraging theoretical results led to a model test program that has demonstrated the control load reduction.

Description of Analysis

The program used for this study is a steady-state aeroelastic rotor analysis that has been under development since 1958. The program uses the transfer matrix method to calculate rotor blade flapwise, chordwise, and torsional deflections and loads together with rotor performance, control system forces, and vibratory hub loads. Articulated, teetering, and hingeless rotors with from 2 to 9 blades and low twist may be analyzed. The analysis is limited to calculations involving steady-state flight conditions at constant rotor tipspeed. The blades may be of arbitrary planform, twist, and radial variation in airfoil section.

The analysis considers coupled flapwise-torsion deflections and uncoupled chordwise deflections of the rotor blade. The blade is represented by 20 lumped masses interconnected in series by elastic elements. The solution is obtained by expanding the variables in a 10-harmonic Fourier series, and the results are iterated between airloads and blade response to account for aeroelastic coupling and nonlinear effects.

Airload calculations include the effects of airfoil section geometry, compressibility, stall, three-dimensional flow, unsteady aerodynamics, and nonuniform inflow. Static airfoil tables are used to account for compressibility, static stall, and airfoil shape. The unsteady aerodynamic loads are calculated by modifying the static loads resulting from the airfoil tables to include expanded Theordor-

Presented as Paper 72-958 at the AIAA 2nd Atmospheric Flight Mechanics Conference, Palo Alto, Calif., September 11-13, 1972; submitted December 1, 1972; revision received November 13, 1973. This paper summarizes work sponsored by the Independent Research and Development Program of the Boeing Vertol Co.

Index categories: VTOL Structural Design (Including Loads); Aeroelasticity and Hydroelasticity; Nonsteady Aerodynamics.

*Manager, Structures Staff.

†Supervisor, Rotor Loads.

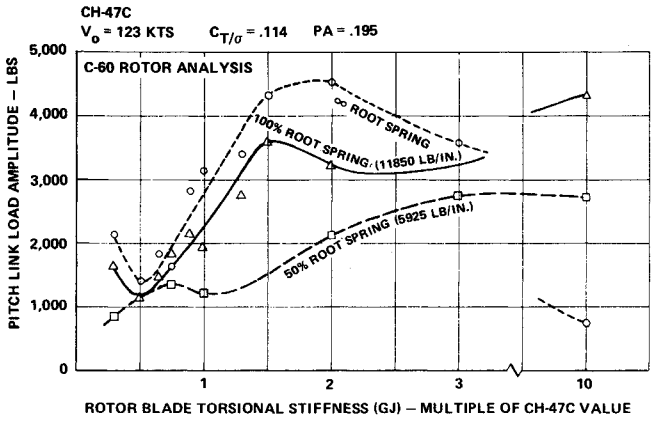

Fig. 1 Variation of pitch link load with rotor blade torsional stiffness.

sen's equations, dynamic stall effects based upon oscillating airfoil two-dimensional test data, and yawed flow. In developing the aerodynamic theory it is assumed that the separate effects of compressibility, dynamic stall hysteresis, and yawed flow can be superimposed to adequately define the unsteady, three-dimensional environment of the helicopter rotor blade. A full discussion of this analysis including correlation with measured flight test data is given in Ref. 5 and a detailed description of the aerodynamic representation is given in the Appendix of Ref. 1.

Analytical Results

What is the effect of blade torsional stiffness, control system stiffness and blade pitch inertia on stall flutter control loads?

To assess the effects of blade torsional stiffness *(GJ)* and control system stiffness *(K_Z)*, an analytical study was run varying both parameters together for a stall flutter flight condition with an airspeed of 123 knots and 0.114 C_T/σ. Three values of control system spring rate were used: ½ the nominal stiffness, nominal stiffness, and infinitely stiff. Eleven values of blade torsional stiffness were used, ranging from 0.30 to 10 times the nominal value. The results of this study show that changes in the stall flutter loads of almost 4 to 1 are possible through these changes (see Fig. 1), but no single clear trend was obtained. Plotting the same results vs torsional natural frequency collapsed the calculated points and led to a simple variation with torsional frequency (see Fig. 2).

To verify the Fig. 2 trend, six different spring rates were analyzed for the nominal blade stiffness. The predicted stall flutter loads fell right in line with the Fig. 2 results further indicating that torsional natural frequency is a principal variable. As a further check, the frequency was varied by changing the blade torsional pitch inertia while maintaining the control system stiffness and blade tor-

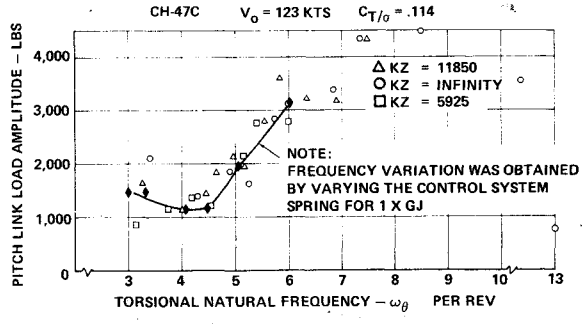

Fig. 2 Stall flutter control load variation vs torsional natural frequency.

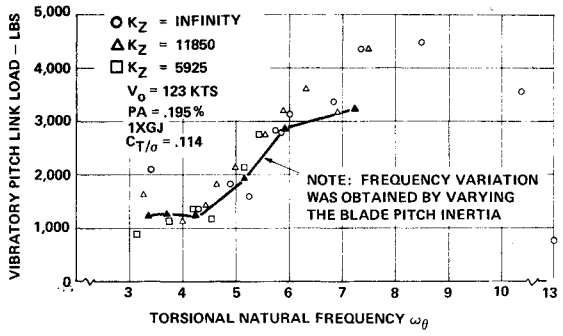

Fig. 3 Stall flutter control load vs torsional natural frequency.

sional stiffness at its nominal values. The results of using six different pitch inertias are shown in Fig. 3, and again these results essentially agreed with previous results as a function of torsional frequency.

All the theoretical results are summarized in Fig. 4 and show that the largest control loads for the analyzed rotor at a C_T/σ = 0.114 and μ = 0.29 occur at torsional natural frequencies between 7/rev and 9/rev. Significantly increasing or decreasing the torsional frequency from the 7 to 9/rev region will reduce the stall flutter control loads. Since many rotor blades have their first torsional natural frequency in the 5 to 7/rev range, stall flutter loads can best be reduced by reducing the torsional frequency. Increasing the torsional frequency to 10/rev or above, with the aim of reducing control loads, appears impractical.

Substantiating Test Results

Model and Test Description

A 6-foot diam model rotor was tested to initially verify that reduced torsional natural frequency reduced stall flutter control loads. The test configuration consisted of a model test stand with a three-bladed hub and three sets of blades. Each blade set had a different torsional natural frequency but identical airfoil section and planform. The first set of blades had a torsional natural frequency of 4.25/rev and was constructed of fiberglass using conventional cross-ply torsion wrap. The second set of blades had mass properties similar to the first blade set, but had a torsional natural frequency of 3.0/rev. These blades were constructed with fiberglass using a uniply torsion wrap, which substantially reduced the blade torsional stiffness. The third set of blades had a torsional frequency of 5.0/rev and was constructed of morganite. Though the morganite blades were not significantly stiffer than the first set of blades, they had significantly lower torsional iner-

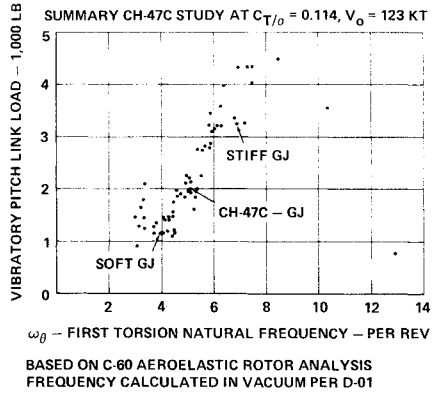

Fig. 4 Influence of rotor blade torsional physical properties on stall flutter pitch link load.

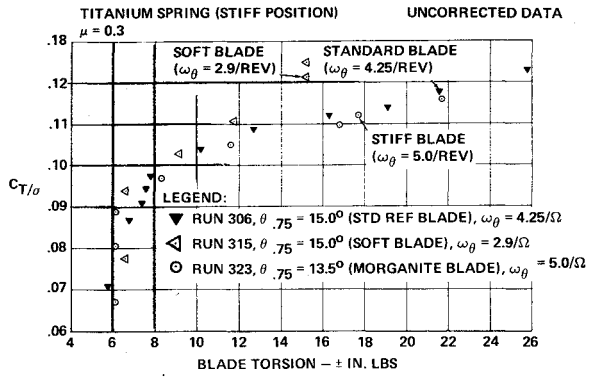

Fig. 5 Torsional loads from 6-ft diam rotor test.

tia, which accounts for the higher torsional natural frequency. The blades were connected to the hub without torsion bearings, and there were no connecting pitch links. This was done so that the blade torsional natural frequency would be known without concern for potential coupling with a dynamic control system. However, this resulted in the loss of cyclic pitch control and a requirement for manual setting of the blade collective.

The lack of cyclic control will clearly modify the blade angle of attack distribution around the azimuth, when compared to a conventional rotor. The effect of forward speed combined with the lack of cyclic pitch causes the rotor tip path plane to blow back, significantly reducing the propulsive force. It is clear that this may modify the way the blade enters the stall region, raising questions as to the applicability of the model results to rotors in conventional flight. It is assumed here that the stall flutter mechanism is fundamental, even for this model rotor configuration, and that the trend of the model results are valid.

The test procedure consisted of setting the collective pitch manually, pointing the rotor shaft approximately 20° into the wind, and bringing the rotor rpm to full-scale tipspeeds (750 fps) at a μ of 0.3. The shaft was then slowly tilted vertically, which increased the rotor C_T/σ. At a C_T/σ of approximately 0.1, the torsion loads would begin growing, indicating the development of stall flutter. It was intended to obtain a nondimensional propulsive force $(\bar{X})$ of about 0.2 in the stall flutter regime, which is typical of actual flight conditions. This was to have been done by performing repeated shaft tilt sweeps at larger collective pitch settings until the desired propulsive forces were obtained.

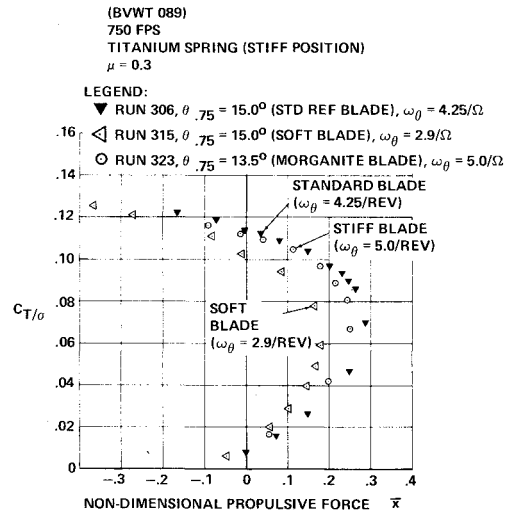

Fig. 6 Propulsive force from 6-ft diam rotor test.

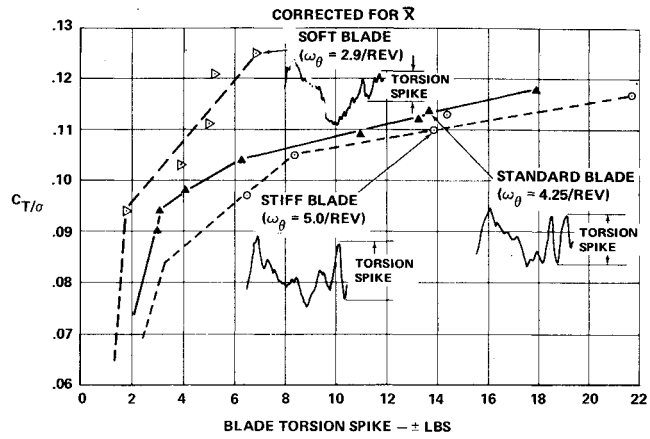

Fig 7 Variation of blade torsion spikes from 6-ft diam rotor test.

However, due to the lack of cyclic pitch, large blade flapping occurred at the high C_T/σ conditions and limited the collective settings through the generation of large chord bending loads and pounding of the up flap stop. The result was that negative propulsive forces were obtained in the stall flutter region, and there were significant differences in propulsive force between the three blade sets at a constant C_T/σ.

Test Results

Figure 5 shows the variation of root torsion load with rotor C_T/σ for the three sets of blades. As shown, the high frequency blade (ω_θ = 5.0/rev) had the largest torsional loads and the softest blade (ω_θ = 3.0/rev), the lowest. This is the raw data without the propulsive force correction that will be described below.

The variation of the propulsive force with C_T/σ is shown in Fig. 6 for the three blade sets and shows large differences in propulsive force in the stall flutter region. Other results obtained for the soft blade and the standard reference blade at different collective pitch settings showed that the torsion loads increased as propulsive force increased at a constant C_T/σ. This conclusion was obtained by cross-plotting torsional load (for runs obtained with various collective angles) vs propulsive force, for a constant C_T/σ. Using these results, the torsion load for the soft blade and standard blade were corrected to agree with the propulsive force of the stiff blade, so that loads can be compared for the same C_T/σ and propulsive force.

Comparison of Model and Full-Scale Results

The variation of blade torsional spike amplitude, corrected for propulsive force, is plotted vs C_T/σ for the three blade sets in Fig. 7. It is clear from the results that

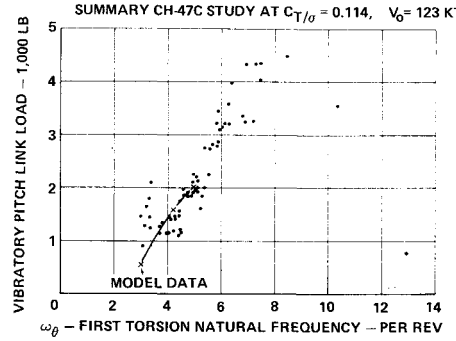

Fig. 8 Comparison of calculated full-scale loads with scaled model data.

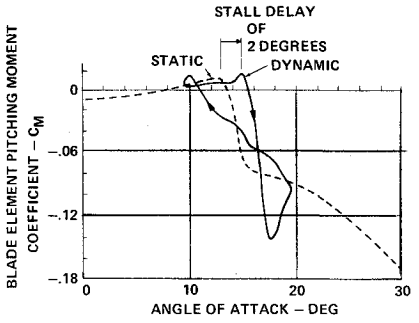

Fig. 9 Comparison of static and dynamic stall.

both analysis and test indicate that a sharp reduction in stall flutter loads are possible by reducing the rotor blades' first torsional natural frequency.

Figure 8 shows model torsional load data scaled up to the calculated full-scale pitch link loads. The scaled loads are proportional to the blade chord squared times the radius. The figure compares this scaled model data with the calculated results discussed above and shows good agreement.

The model data must be considered with care since: 1) realistic propulsive forces (typical of aircraft forward speed flight) were not obtained due to test configuration limitations; 2) lack of data at constant propulsive force and thrust for each blade stiffness introduced a potential source of error, since the data was corrected to obtain consistent propulsive forces among the different blades; and 3) a large 1/rev component of the model waveform, which was frequently larger than the stall spike, partially obscured the load picture.

What is the Stall Flutter Mechanism?

Sequence of Events for a 2-D Airfoil Section

To understand the stall flutter mechanism, the sequence of events for an airfoil section will be examined as it proceeds around the rotor azimuth. The aim of this exercise will be to investigate the causes of the high-frequency "stall flutter" loads and try to understand why these loads are sensitive to torsional natural frequency.

As a rotor blade traverses the rotor azimuth, the velocity varies around the disc because of advance ratio effects. The velocities are large for the advancing blade and small for the retreating blade. Conventional helicopters cannot carry large steady hub rolling moments; therefore, the advancing blade lift moment approximately equals the retreating blade lift moment. The moment balance implies that the advancing and retreating blade lifts are roughly equal, which requires the retreating blade to have a larger angle of attack to make up for the low relative wind velocity in this region. As rotor thrust, propulsive force, or advance ratio increase, so must the retreating blade angle of attack—until eventually the angle of attack exceeds the static stall angle, leading to airoil section stall.

When an airfoil section stalls, large changes occur in the section lift and pitching moment. However, the angle of attack at which stall occurs and the nature of the airload change differ greatly between static and pitching airfoils. Figure 9 compares static stall data (i.e., variation of C_M for fixed airfoil angles of attack) with dynamic stall data[3] (i.e, obtained for airfoils oscillating in pitch). The figure clearly shows a dynamic stall delay of two degrees when compared to static data. Also shown is an *un*stall delay of approximately the same magnitude.

Rotor blade behavior is far from that of a static airfoil, since the rotor blade angle of attack experiences rapid changes due to pitch and flapping motion, nonuniform downwash and large changes in tangential velocity. It has been found from experiments[4] that the dynamic stall delay is proportional to the square root of the airfoil pitch rate ($\dot{\alpha}$). Therefore, the rotor blades rapid changes in airfoil angle of attack can cause significant stall delay and large changes in the airfoil lift and pitching moment. Using static airfoil data to calculate the rotor blade behavior can be very misleading when significant blade stall is present.

To investigate the stall flutter mechanism, the dynamic stall-*un*stall cycle will be examined for a blade segment rotating around the azimuth. Assume that the conditions are such that in the retreating portion of the blade azimuth, the airfoil section angle of attack exceeds that static stall angle, and the angle of attack is increasing; i.e., $\dot{\alpha}$ is positive. When this occurs, dynamic stall delay results, and the pitching moment variation continues as before, with no stall and no large changes. As the angle of attack amplitude (α) reaches its maximum value, its time derivative (α) reduces. Before $\dot{\alpha} = 0$ (i.e., $\alpha = \alpha_{max}$), the values of $\dot{\alpha}$ is insufficient to delay stall any longer and stall occurs.

At approximately the same time that stall occurs, the airfoil section reaches its maximum nose-up deflection (i.e., at $\dot{\alpha} = 0$). Therefore, just as a large nose-down pitching moment is generated by the stalling mechanism, the blade begins to pitch nose down. The large nose-down pitching moment is in phase with the nose-down motion resulting in work being performed by the air on the blade. Through this portion of the cycle, $\dot{\alpha}$ is negative; and, when the angle of attack passes below the static stall angle, an *un*stall delay occurs. Blade *un*stall occurs just before $\dot{\alpha} = 0$ (i.e., $\alpha = \alpha_{min}$) from the negative side. A large nose-up change in pitching moment occurs just as the blade is about to pitch nose up. Again the blade motion and the pitching moment changes are in phase, and the air does work on the airfoil. This stall delay-*un*stall delay cycle continues almost in phase with the blade motion, pumping energy from the air to the blade until the angle of attack achieved on the up stroke is insufficient to reach the static stall angle.

Effects of Stall Radial Distribution and Flexibility

The preceding discussion considered the dynamic stalling mechanism of a single isolated airfoil section and has

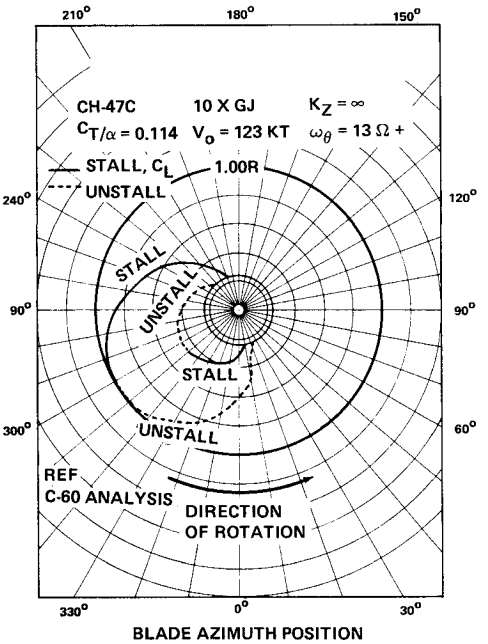

Fig. 10 Dynamic stall variations with blade azimuth and radius for frequency of 13/rev.

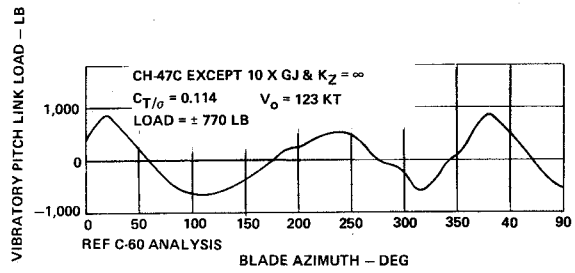

Fig. 11 Pitch link load waveform for a torsional natural frequency of 13/rev.

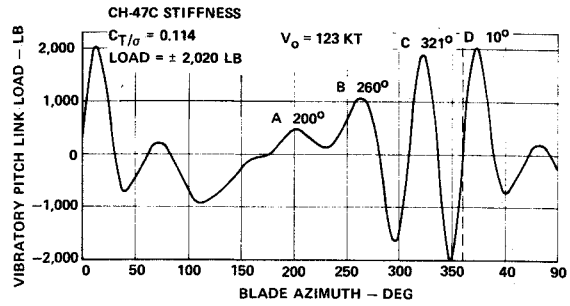

Fig. 13 Pitch link load waveform for a torsional natural frequency of 5.2/rev.

not investigated the impact of the spanwise load distribution or the effect of blade flexibility. To determine these effects, pitch-link load waveforms and stall polar plots have been studied for a torsionally rigid blade and a flexible blade.

For the rigid blade, the stall distribution is spread throughout the blade azimuth (Fig. 10). At 60% span, the blade stalls at an azimuth position of 239°; at the blade tip, stall occurs at an azimuth position of 300°. The effect of this distributed stall on the pitch-link-load waveform is shown clearly in Fig. 11 as a gradual nose-down pitching moment occurring from an azimuth of 240° to 315°.

For a torsionally flexible blade with a torsional natural frequency of 5.2/rev (Fig. 12), large portions of the blade stall simultaneously. The portion of the blade from 65% to the cutout stalls at approximately 200° azimuth (stall A), the outboard 40% of the blade stalls at 260° azimuth (stall B), virtually the whole blade stalls at 320° azimuth (stall C), and finally, the inboard 65% stalls at 10° azimuth (stall D). Each time a portion of the blade experiences simultaneous stall over a large portion, the pitch-link load waveform experiences a nose-down pitching moment (as shown in the Fig. 13 waveform). The nose-down stall pitching moment is larger for the flexible blade than for the rigid blade, since the flexible blade stalls simultaneously over large portions of the blade, causing a large step loading on the blade, while the rigid blade loading is applied gradually.

It is this simultaneous stall over a significant portion of the blade that provides the large nose-down stall spikes in the pitch-link-load waveform. The resulting energy flow from the air to the blade (negative damping) increases the elastic deflections. The resulting elastic blade twist may lead to one or more additional submersions into and out of stall with the large nose-down pitching moment following.

Torsional flexibility plays a decisive role in the development of simultaneous stall. To understand the influence of torsional deflection on dynamic stall, one must recognize that before an airfoil section dynamically stalls, the angle of attack is above the static stall angle, and a positive pitch rate is delaying stall. A nose-down pitching moment introduced by inboard section stalling causes the positive pitch rate (nose up) to reduce, causing the adjacent section to stall. Therefore, simultaneous stall results from coupling deflections from one blade spanwise element to the next. When a flexible blade section stalls, it pulls the adjacent section along, spreading down the blade span until a significant portion of the blade experiences simultaneous stall.

From the above discussion it is clear that blade stiffness can be expected to significantly affect stall flutter loads. Also from the discussion it is expected that very stiff blades, with small elastic deflections, would result in low stall flutter loads. However, the finding of low torsional loads at the low-frequency (low stiffness) region comes as a surprise.

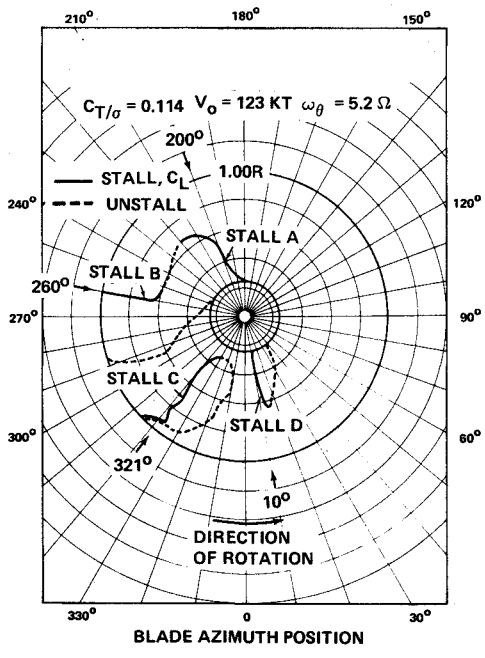

Fig. 12 Dynamic stall variation with blade azimuth and radius for frequency of 5.2/rev.

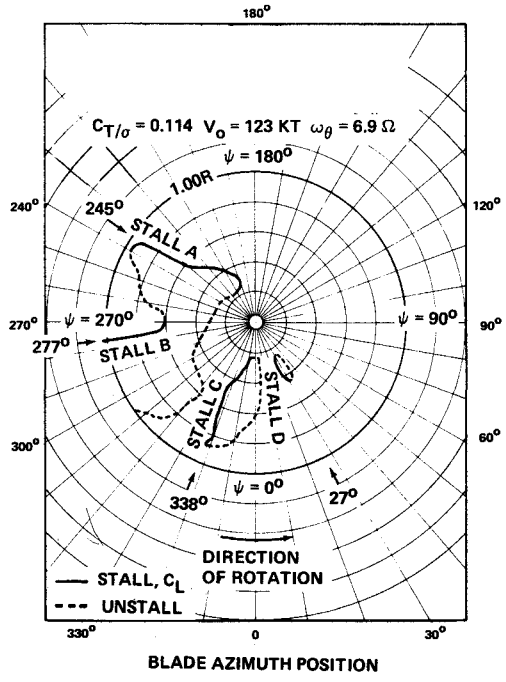

Fig. 14 Dynamic stall variation with blade azimuth and radius for frequency of 6.9/rev.

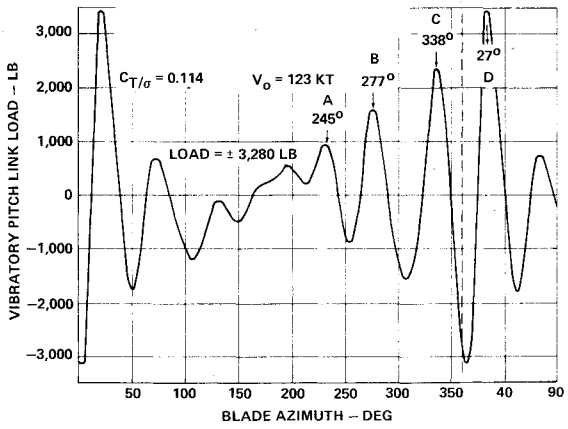

Fig. 15 Pitch link load waveform for a torsional natural frequency of 6.9/rev.

Why Does a Low Value of Torsional Natural Frequency Result in Reduced Control Loads?

When the torsional natural frequency of the blade is changed, the flexible response to the nose-down stall step varies. Figures 14–17 present pitch-link-load waveforms and stall polar plots for a relatively stiff blade with a torsional natural frequency of 6.9/rev, and a relatively soft blade with a torsional natural frequency of 4.0/rev. The stiffer blade (6.9/rev) exhibits larger regions of simultaneous stall and larger pitch-link loads than the basic blade (5.2/rev). The soft blade (4.0/rev) shows smaller regions of simultaneous stall and reduced pitch-link loads.

These plots indicate that the stiffer blade (ω_θ = 6.9/rev) was more efficient in generating a stall-unstall cycle over a significant portion of the blade than the softer blade (ω_θ = 4.0/rev). This occurred even though the stiffer blade would have a lower static deflection than the soft blade. Therefore, the explanation must lie with the dynamic response of the blade.

Figure 18 compares the frequency of the stall flutter torsional load spikes with the blade torsional natural frequency for all the analytical data points that displayed stall flutter waveforms. The stall flutter frequency varies

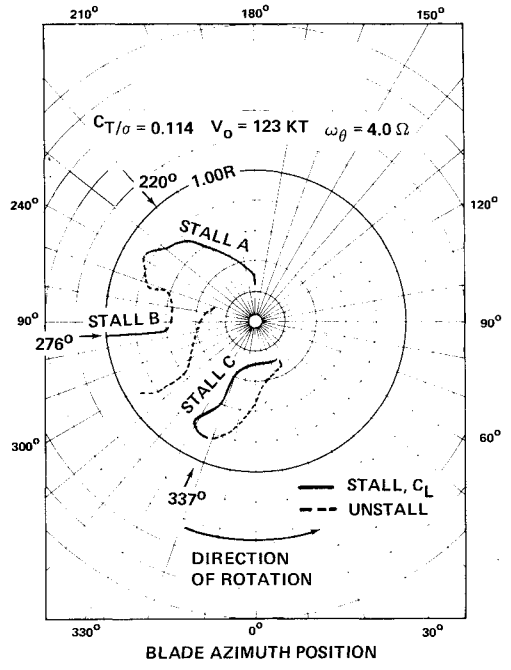

Fig.16 Dynamic stall variation with blade azimuth and radius for frequency of 4.0/rev.

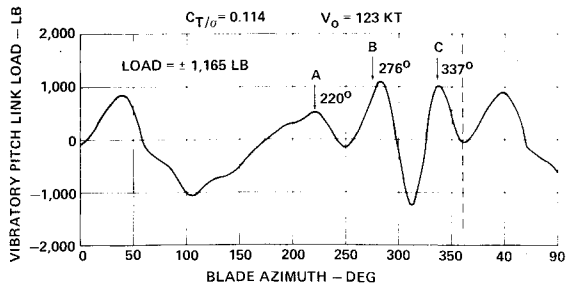

Fig. 17 Pitch link load waveform for a torsional natural frequency of 4.0/rev.

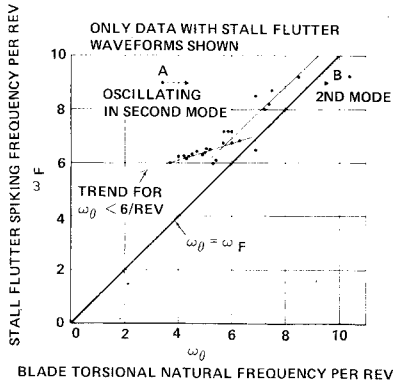

Fig. 18 Comparison of stall flutter spiking frequency with blade torsional freqency.

from 6/rev to 9.2/rev, while the blade torsional natural frequency varies from 3.7/rev to 10.4/rev. For blades with torsional natural frequencies below 3.7/rev, stall flutter-type waveforms were not present‡ and therefore these points were not included on the figure.

From Fig. 18, it appears that the stall flutter mechanism is forcing the blade at frequencies between 6/rev and 9/rev, and the blade is simply responding to this external forcing. Therefore, when the forcing frequency and the natural frequency become close, the amplification factor increases and so do the torsional loads.§ Conversely, when the forcing frequency is significantly removed (2.0/rev or greater) from the blade natural frequency, little amplification of the torsional elastic deflections result; and only a small elastic deflection is available to feed the stall flutter mechanism; hence, no significant control loads are developed.

Possibly, the stall flutter airload forcing frequencies are associated with the limited azimuth region for which stall can occur. For a rotor in forward flight, the advancing blade has small angles of attack, while the retreating blade has large angles of attack. For a given flight condition, a rigid blade angle of attack distribution would show areas of the rotor disc where α exceeds the static stall angle, areas where α is a few degrees below the static stall angle and areas where α is far below static stall. The first

‡There is one analytical data point (point A on Fig. 18) where a stall flutter waveform was present for a torsional natural frequency below 3.7/rev. This blade had a torsional natural frequency of 3.4/rev and a stall flutter frequency of 9/rev. However, the blade's second torsional natural frequency was 9.4/rev, and the blade was probably oscillating in its second mode. Therefore, point A was transferred to point B where it fell in line with all the previous data.

§The control load vs torsional natural frequency curve (Fig. 4) looks like a simple forced response curve where the response peaks when the forcing frequency and system natural frequency coincide. The large response for the 3.4/rev blade represents a secondary peak due to the coincidence of the forcing frequency and second-mode frequency.

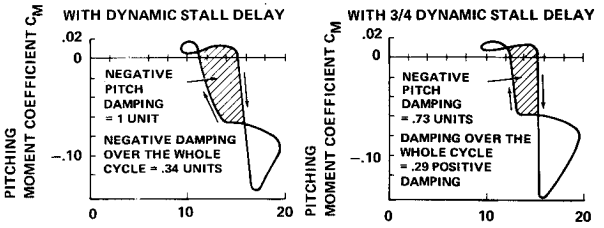

Fig. 19 Reduction of negative pitch damping due to a reduction of dynamic stall delay.

two areas compose a potential stall flutter region where significant elastic deflections can generate the required stall-unstall cycles that lead to stall flutter. It appears that for a given stall flutter region, a specific number of stall-unstall cycles are required to extract the maximum energy from the air.

If the stall flutter oscillations occur at a low frequency, the number of stall-unstall cycles is reduced. In addition, the pitch rate, $\dot{\alpha}$, is reduced resulting in a reduction of the dynamic stall delay. The effect of reducing the dynamic stall delay is illustrated in Fig. 19. A one-quarter reduction in the dynamic stall delay reduces the energy inflow from the air by 27%. Therefore, for low-frequency torsional oscillation, the combination of reduced air-induced energy per stall-unstall cycle, and a reduced number of cycles, results in a significant reduction of the net energy flow into the blade. This suggests that it is possible that a blade with a low torsional natural frequency could obtain more energy input from the air if it oscillates at a higher frequency.

If the oscillating frequency becomes very large, the available stall delay increases; but the elastic amplitude decreases, resulting eventually in: 1) Elastic angles of attack too small to enter stall, and 2) A lack of simultaneous stall buildup resulting in distributed stall, as shown in Fig. 10, for a torsionally rigid blade. Currently, this mechanism has not been fully investigated, since it involves tradeoffs between elastic pitch amplitude, stall delay (or $\dot{\alpha}$) and the number of stall cycles.

Conclusions

The results presented show that a rotor blade's torsional natural frequency plays a major role in determining stall flutter loads. A reduced blade torsional frequency results in substantially lower torsional loads. The discoveries here open a promising avenue into a possible method for reducing these loads for the next generation helicopter. However, it remains to be shown how the stall flutter loads change with flight condition and rotor configuration, and significant future investigations remain. These include:

1) Correlation of the aeroelastic theory with the existing model rotor test data for blades with different torsional natural frequencies.

2) An expanded analytical study to investigate the influence of blade torsional properties over a wide range of flight conditions on blade stall-induced torsional loads.

3) A model test of rotor blades with different torsional natural frequencies, using cyclic pitch control, over a wide range of flight conditions to fully represent the actual rotor flight environment.

4) An expanded understanding of the stall flutter mechanism to allow exploration of all means for reducing or eliminating these torsional loads.

References

[1]Tarzanin, F. J., Jr., "Prediction of Control Loads Due to Blade Stall," Presented as Paper 513 at the 27th Annual National Forum of the American Helicopter Society, May 1971, Washington, D.C.

[2]Carta, F. O. et al., "Analytical Study of Helicopter Rotor Stall Flutter," Presented as Paper 413 at the 26th Annual National Forum of the American Helicopter Society, June 1970, Washington, D.C.

[3]Liiva, J., Davenport, F. et al., "Two-Dimensional Tests of Airfoils Oscillating Near Stall," USAAVLABS Tech. Rept. 68-131A, 1968, U.S. Army Aviation Material Labs., Fort Eustis, Va.

[4]Gross, D. and Harris, F., "Prediction of Inflight Stalled Airloads from Oscillating Airfoil Data," Presented as Paper 322 at the 25th Annual National Forum of the American Helicopter Society, May 1969, Washington, D.C.

[5]Gabel, R. "Current Loads Technology for Helicopter Rotors," AGARD, April 1973.